An empirical potential energy surface for $He–Cl_2(B\,^3\Pi_u)$ based on a multiproperty fit

Cite as: J. Chem. Phys. **119**, 5583 (2003); https://doi.org/10.1063/1.1599342
Submitted: 02 May 2003 . Accepted: 18 June 2003 . Published Online: 28 August 2003

A. García-Vela

An empirical potential energy surface for $He–Cl_2(B\,^3\Pi_u)$ based on a multiproperty fit

A. García-Vela[a)]
Instituto de Matemáticas y Física Fundamental, C.S.I.C., Serrano 123, 28006 Madrid, Spain

(Received 2 May 2003; accepted 18 June 2003)

An empirical interaction surface for the $He–Cl_2(B\,^3\Pi_u)$ complex based on additive pairwise potentials is reported. A novelty of the present surface with respect to previous empirical potentials is that a dependence on the Cl–Cl separation is introduced in some of the potential parameters, which makes more flexible the analytic form used. The parameters of the surface are adjusted in order to reproduce the available data for several properties such like spectral blueshifts, predissociation lifetimes, and Cl_2 product state distributions. The fitted surface yields very good agreement with experiment for most of the properties measured. As compared with previous surfaces, the present potential is found to improve significantly on the description of the vibrational dependence of the lifetime, in all the range of vibrational excitations probed by the experiment. In previous works this property has revealed difficult to describe accurately for $He–Cl_2(B)$. For the remaining properties, the current surface provides a level of accuracy as good (or better in some cases) as the best one achieved by earlier interaction potentials. The features of the proposed potential surface and its range of validity are discussed. It is found that validity of the potential is essentially limited to the range of vibrational levels probed experimentally. © *2003 American Institute of Physics.* [DOI: 10.1063/1.1599342]

I. INTRODUCTION

The characterization of the potential-energy surfaces of rare gas–dihalogen van der Waals (vdW) complexes has received a great deal of attention in the last years. Empirical[1–5] and *ab initio*[4,6–18] potential surfaces have been reported for several complexes like $He–Cl_2$, $Ne–Cl_2$, $Ar–Cl_2$, $Ne–I_2$, $Ar–I_2$, for both the ground and excited electronic states. The availability of accurate spectroscopic and dynamical experimental data makes possible to test the potential surfaces proposed, and has motivated much of this research effort. Among the vdW complexes investigated, $He–Cl_2$ has been one of the most extensively studied. Several potential surfaces have been proposed for the ground electronic state $He–Cl_2(X\,^1\Sigma_g)$.[2,3,6–12] The excited electronic state $He–Cl_2(B\,^3\Pi_u)$ has also been the subject of a number of works which have generated both empirical[2,3] and *ab initio* or *ab initio*-based surfaces.[7,12–14]

The $He–Cl_2$ $B(v')\leftarrow X(v''=0)$ transition has been probed experimentally in the region $v'=6-12$.[2,3,14,19] Spectroscopic data such as excitation spectra and blueshifts of the $He–Cl_2$ $B(v')\leftarrow X(v''=0)$ band origins from the corresponding Cl_2 $B(v')\leftarrow X(v''=0)$ band origins were measured. Upon vibrational predissociation (VP) of the complex in the excited electronic state, predissociation lifetimes and product state distributions of the $Cl_2(B,v<v')$ fragment were also obtained. The empirical potentials for the $He–Cl_2(B)$ state[2,3] were fitted to these experimental data. In general good agreement with observations was obtained for the blueshifts and the vibrational and rotational $Cl_2(B,v<v')$ distributions. Concerning the VP lifetime, agreement with experiment was less good. The lifetime was overestimated for the higher vibrational levels $v'=11$, 12, and underestimated for the lower levels $v'<10$.

The first *ab initio* surface for the $He–Cl_2(B)$ state tested with the experimental data was calculated at the fourth-order unrestricted Møller-Plesset (UMP4) level of theory, and corrected with *ab initio* points at the unrestricted coupled-cluster level with single and double (triple) configurations [UCCSD(T)] level.[7] Again excitation spectra and product state distributions were generally well reproduced by this surface. However, the spectral blueshifts obtained were too short as compared to experiment, and the VP lifetimes were similar (slightly improved) as those found with the empirical[2,3] potential surfaces. In a further work, an *ab initio* surface for $He–Cl_2(B)$ calculated at the UCCSD(T) level was reported.[14] The description of the spectral blueshifts with the UCCSD(T) surface was remarkably improved with respect to the UMP4 one, and discrepancies with experiment ranged between 3% and 12%. State distributions of the $Cl_2(B)$ fragment were reproduced with similar accuracy as with the previous empirical and corrected UMP4 surfaces, and the calculated excitation spectra exhibited the experimental structure, although peak intensities agreed less with experiment than in the case of the corrected UMP4 surface. The VP lifetimes obtained with the UCCSD(T) surface compared very well with the measured ones for $v'=11$, 12, but they were too short (even shorter than with previous surfaces) for lower vibrational levels.

In the same study,[14] the authors carried out a fit of the UCCSD(T) surface using a microgenetic algorithm (μGA). The adjusted μGA surface typically improved on the de-

a)Electronic mail: garciavela@imaff.cfmac.csic.es

scription of the measured observables, and in particular of the spectral blueshifts, which were now reproduced within experimental precision (~1% of discrepancy with experiment). The VP lifetimes for the lower $v'=8-10$ levels were clearly improved with respect to the UCCSD(T) surface, and somewhat better than those obtained with the earlier empirical and corrected UMP4 surfaces. Part of the improvement of the μGA surface in describing the $v'=8-10$ lifetimes was made, however, at the expense of the $v'=11$, 12 lifetimes, which were predicted to be too long. Taking into account the global comparison with experiment of all the spectroscopic and dynamical magnitudes reproduced, the semiempirical, *ab initio*-based μGA surface can be considered as the most reliable potential surface for the excited $He-Cl_2(B)$ state reported so far.

At present, existing $He-Cl_2(B)$ potential surfaces describe well (or even very accurately, as the blueshifts obtained from the μGA surface) most of the observables measured in the range $v'=6-12$ of vibrational excitations. The clear exception is the VP lifetime, whose quality of description by the current surfaces is still significantly lower than that of other spectroscopic and dynamical quantities. A reasonable description of the lifetime for the higher $v'=11$, 12 vibrational levels typically involves to underestimate the lifetime of the lower levels $v'<10$, while when the lifetime for the lower levels is well reproduced the lifetime corresponding to the higher vibrations is too overestimated. The difficulty in reproducing the experimental VP lifetime of $He-Cl_2(B)$ in the entire range $v'=8-12$ has been previously discussed.[2,3,14] Its origin has been related to the large amplitude motions undergone by the He atom, which samples potential regions that largely affect the lifetime and need a precise characterization. The aim of the present work is to propose an empirical potential surface for $He-Cl_2(B)$ which significantly improves on the description of the VP lifetime in the $v'=8-12$ range of vibrational levels. The goal is to obtain such an improvement while still keeping at least the best quality of description achieved by the previous surfaces for the remaining properties measured.

The organization of the paper is the following. In Sec. II the potential-energy surface proposed is described, and the details of the calculations carried out to reproduce the magnitudes observed experimentally are given. Results are shown and compared to those obtained with previous potential surfaces in Sec. III. The important point of the validity limits of the present empirical potential is also analyzed and discussed in this section. Some conclusions are given in Sec. IV.

II. THEORETICAL METHOD

A. Potential-energy surface

The modeling of empirical potential surfaces for the B electronic state of rare gas–dihalogen vdW complexes has been commonly based on additions of pairwise interactions. A sum of atom–atom Morse potentials recently fitted to experimental data for the $Ne-I_2(B,v')$ surface, was shown to give a reliable description of the spectroscopy and dynamics over a wide range of v' vibrational excitations.[5] Similarly, empirical surfaces for $Ne-Cl_2(B)$ consisting of additive atom–atom potentials to describe the hard wall and the well of the $Ne-Cl_2$ interaction, and smoothly connected to a long-range vdW attraction,[20] have provided good agreement with experiment.[1,21] Functional forms similar to that suggested for $Ne-Cl_2(B)$,[20] with some modifications, were used to model the earlier empirical surfaces for $He-Cl_2(B)$.[2,3] The main advantage of this type of potential forms is that they are relatively simple functions with few parameters to adjust.

TABLE I. Potential parameters and atomic masses used in this work.

$D=3145.0\ cm^{-1}$	$a_2=0.607\ Å^{-3}$
$\beta=2.353\ Å^{-1}$	$r^*=2.907\ Å$
$r_e=2.414\ Å$	$x_m=3.77\ Å$
$\epsilon_0=14.52\ cm^{-1}$	$m_{Cl}=35.453$ a.m.u.
$\alpha_0=1.439\ Å^{-1}$	$m_{He}=4.003$ a.m.u.
$a_1=5.357\ cm^{-1}\ Å^{-2}$	

The $He-Cl_2$ system is represented in (r, R, θ) Jacobian coordinates, where r is the Cl–Cl bond length, R is the distance between He and the Cl_2 center-of-mass, and θ is the angle between the vectors **r** and **R** associated with the two radial coordinates. Then, as in previous works[2,3] the $He-Cl_2(B)$ surface is modeled as

$$V(r,R,\theta)=V_{Cl_2}(r)+V_{int}(r,R,\theta), \tag{1}$$

where $V_{Cl_2}(r)$ is the intramolecular Cl–Cl potential in the B electronic state, and $V_{int}(r,R,\theta)$ describes the $He-Cl_2(B)$ intermolecular interaction. The V_{Cl_2} term is represented by a Morse function

$$V_{Cl_2}(r)=D[e^{-2\beta(r-r_e)}-2e^{-\beta(r-r_e)}], \tag{2}$$

whose parameters[21] are listed in Table I. This potential is slightly different from the RKR potential used for Cl_2 in Refs. 2 and 3. The functional form for the $V_{int}(r,R,\theta)$ term is a sum of two Morse potentials describing the two He–Cl interactions, respectively,

$$V_{int}(r,R,\theta)=\epsilon(r)\sum_{i=1}^{2}[\{1-\exp[-\alpha(r)(x_i-x_m)]\}^2-1], \tag{3}$$

where x_i denotes the He–Cl distances

$$x_{1,2}^2=\frac{r^2}{4}+R^2+rR\cos(\theta), \tag{4}$$

and x_m is the position of the Morse potential minimum.

The main novelty of the present $He-Cl_2(B)$ intermolecular potential $V_{int}(r,R,\theta)$ is that an explicit r dependence has been introduced in the Morse parameters $\epsilon(r)$ and $\alpha(r)$ for the He–Cl interaction. The explicit dependence of some of the He–Cl potential parameters on the Cl–Cl distance introduces a three-body character in the $He-Cl_2$ intermolecular potential, and makes it more flexible. The idea of incorporating a dependence on the Cl–Cl distance in some of the $He-Cl_2(B)$ potential parameters was previously suggested,[3] and applied in the analytical potential surface fitted to the UMP4 *ab initio* points calculated in Ref. 7. The result that the VP lifetimes obtained with that surface agreed

better with experiment that those computed with the higher level UCCSD(T) one was attributed in part to the dependence on the Cl–Cl separation. Clearly, it would be desirable to carry out high level *ab initio* calculations with enough density of points, particularly in the Cl–Cl separation, as to obtain a surface which accurately describes the delocalized situation of the He–$Cl_2(B)$ complex. Such calculations, however, are very time consuming. In the absence of these calculations, improving on existing He–$Cl_2(B)$ empirical potentials becomes a realistic alternative, and introducing a dependence of the potential parameters on the Cl–Cl separation appears as a sensible way to achieve that improvement.

The choice of a functional form for $\epsilon(r)$ and $\alpha(r)$ is far from being obvious, and therefore it is rather arbitrary. However, by considering some physical features of the Cl–Cl potential and its vibrational states, one can model simple functional forms for $\epsilon(r)$ and $\alpha(r)$. The goal is to reproduce the dependence observed experimentally for different properties on the Cl_2 vibrational excitation. Due to the anharmonicity of the Cl–Cl potential, the Cl_2 vibrational states become increasingly different in the region of the Cl–Cl separation corresponding to the outer turning point. As v' increases, population of the vibrational state shifts gradually toward larger Cl–Cl distances. These differences between the Cl_2 vibrational states can be exploited in order to model the r dependence of $\epsilon(r)$ and $\alpha(r)$, such that the vibrational dependence of the measured quantities is reproduced.

The above discussion suggests that $\epsilon(r)$ and $\alpha(r)$ should vary in the region of larger Cl–Cl separations where the vibrational states become more different, while $\epsilon(r)$ and $\alpha(r)$ can remain constant in the region of the Cl_2 potential well, where the vibrational states are more similar in shape. Simple functional forms for $\epsilon(r)$ and $\alpha(r)$ fulfilling these requirements are

$$\epsilon(r)=\epsilon_0 \quad \text{if } r\leqslant r^*, \tag{5a}$$

$$\epsilon(r)=\epsilon_0-a_1(r-r^*)^2 \quad \text{if } r>r^* \tag{5b}$$

and

$$\alpha(r)=\alpha_0 \quad \text{if } r\leqslant r^*, \tag{6a}$$

$$\alpha(r)=\alpha_0-a_2(r-r^*)^2 \quad \text{if } r>r^*. \tag{6b}$$

The relevant parameters used in Eqs. (5) and (6) (along with the remaining potential parameters) are listed in Table I. In Fig. 1 the behavior of $\epsilon(r)$ and $\alpha(r)$ is displayed in the r range populated by the Cl_2 vibrational states $v'\leqslant 12$. The wave functions of the $v'=8$ and $v'=12$ vibrational states are also shown in the figure to illustrate how they change in shape in the region of larger Cl–Cl separations. Both $\epsilon(r)$ and $\alpha(r)$ are constant up to $r=2.91$ Å, and then they decrease monotonically in the region $r>2.91$ Å, where vibrational population gradually concentrates as v' increases from $v'=8$ to $v'=12$. It should be noted that the variation with the Cl–Cl separation of the ϵ and α parameters is not independent, but closely connected. Otherwise it is not possible to reproduce simultaneously the spectral blueshift and the VP lifetime over a range of several Cl_2 vibrational levels. It is also worth noting that the present He–$Cl_2(B)$ intermolecular potential has a simple analytical form involving only 6 parameters.

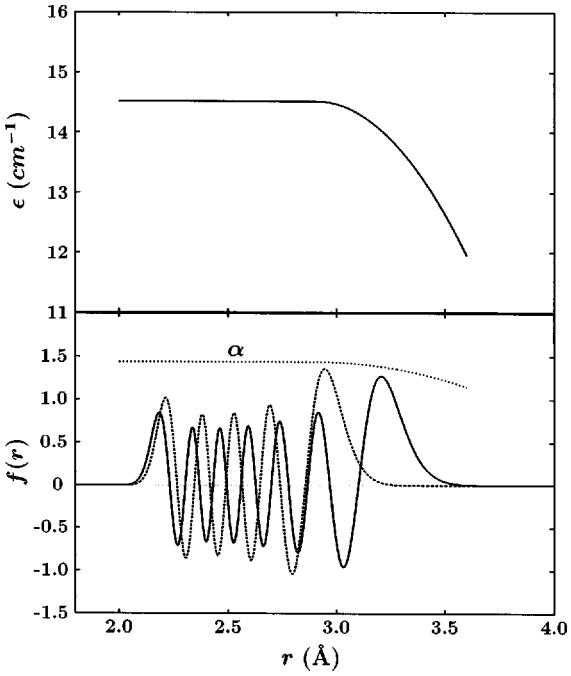

FIG. 1. Behavior of the ϵ and α (in $Å^{-1}$) functions of Eqs. (5) and (6) vs the Cl–Cl distance r. The Cl_2 vibrational wave functions $\chi_{v'}^{(j=0)}(r)$ are also shown in the lower panel for $v'=12$ (solid line) and $v'=8$ (dashed line).

B. Spectroscopic and dynamical calculations

The ϵ_0, α_0, a_1, a_2, r^*, and x_m parameters of the He–$Cl_2(B)$ intermolecular potential were fitted in order to reproduce the measured values of several spectroscopic and dynamical observables in the range $v'=6-12$ of Cl_2 vibrational excitations. Such experimental data include the spectral blueshifts for the $v'=8-12$ band origins; the VP lifetimes of the $v'=8-12$ levels; the $\Delta v'=-1$ Cl_2 product rotational state distributions for predissociation from $v'=6$, 8, 10; the $\Delta v'=-1$, -2, and -3 product rotational distributions for predissociation from $v'=12$; and the Cl_2 vibrational distribution for dissociation from $v'=12$. In the following, details of the calculations of these quantities are described.

The blueshift of the He–Cl_2 $B(v')\leftarrow X(v''=0)$ band origins from the corresponding Cl_2 $B(v')\leftarrow X(v''=0)$ band origins is obtained as $D_0(X)-D_0(B)$. It is considered that the best potential surface currently available for He–$Cl_2(X)$ is the *ab initio* surface of Ref. 11. The dissociation energy obtained with this surface is $D_0(X)=14.85\ cm^{-1}$, and this is the value used in the present work. The dissociation energy $D_0(B)$ for a vibrational level v' coincides with the energy of the ground resonance state of the He–$Cl_2(B,v')$ complex. In order to calculate this resonance energy, the resonance wave function is expressed as

$$\Phi(r,R,\theta)=\sum_{n,j} c_{n,j}^{(v)}\psi_n^{(v)}(R)\chi_v^{(j)}(r)P_j(\theta), \tag{7}$$

where $\chi_v^{(j)}(r)$ are the rovibrational eigenstates of the Cl_2 molecule, $P_j(\theta)$ are normalized Legendre polynomials, and $\psi_n^{(v)}(R)$ are radial basis functions. The radial functions are obtained by calculating the eigenfunctions of the reduced Hamiltonian $\hat{H}_{vv}(R,\theta)=\langle\chi_v^{(j=0)}(r)|\hat{H}|\chi_v^{(j=0)}(r)\rangle$ [where $\hat{H}$ is the full Hamiltonian of He–$Cl_2(B)$] for several fixed angles θ, and then orthogonalizing these eigenfunctions through the Gram–Schmidt procedure. By representing the Hamiltonian $\hat{H}$ in the basis set of Eq. (7) and diagonalizing, the resonance energy and wave function are obtained. Since the vibrational mixing of the $\chi_v^{(j)}$ states is quite small for this type of systems,[5,21] only one vibrational state, $v=v'$, was included in the basis set. It was found that 10 $\psi_n^{(v)}$ radial functions and 15 Legendre polynomials (with even j) lead to converged resonance energies.

The predissociation dynamics of the complex ground resonance state, $He–Cl_2(B,v')\rightarrow He+Cl_2(B,v<v')$ is simulated by solving the time-dependent Schrödinger equation for the wave packet $\Phi(r,R,\theta,t)$. To this purpose the wave packet is expanded as

$$\Phi(r,R,\theta,t)=\sum_{v,j} C_{v,j}(R,t)\chi_v^{(j)}(r)P_j(\theta)e^{-E_v^{(j)}t/\hbar}, \qquad (8)$$

where $E_v^{(j)}$ are the energies associated to the $\chi_v^{(j)}$ states. The expansion coefficients $C_{v,j}(R,t)$ are the packets which are actually propagated through a set of time-dependent coupled equations. These packets were represented on a uniform grid in the R coordinate consisting of 128 points with $R_0=3.0$ a.u. and $\Delta R=0.25$ a.u. In the expansion of Eq. (8) four vibrational states corresponding to $v=v'$, $v'-1$, $v'-2$, $v'-3$, and 15 rotational states (with even j) were included for all the dynamical calculations. The wave packet was absorbed before reaching the edges of the grid in the R coordinate. Absorption was carried out after each propagation time step by multiplying each packet $C_{v,j}(R,t)$ by the function $\exp[-A(R-R_{abs})^2]$, for $R>R_{abs}$, with $A=0.5$ a.u.$^{-2}$ and $R_{abs}=28.0$ a.u.

The time propagation of the $C_{v,j}(R,t)$ packets was carried out using the Chebychev polynomial expansion method[22] to express the evolution operator. A propagation time step $\Delta t=0.04$ ps was applied. The wave packet was propagated until a final time $t_f=20$, 28, 36, 44, 52, and 64 ps for the vibrational levels $v'=12$, 11, 10, 9, 8, and 6, respectively. The time evolution of the square of the wave packet autocorrelation function $P(t)=|\langle\Phi(0)|\Phi(t)\rangle|^2$ was calculated. As it has been shown,[23] by propagating the wave packet until a final time t_f, one can obtain the autocorrelation function until a time $2t_f$. The procedure used here to calculate the autocorrelation function until a time $2t_f$ has been described in detail elsewhere.[24] By fitting the decay curve $P(t)$ to an exponential law $P(t)\simeq e^{-t/\tau}$, the predissociation lifetime τ of the $He–Cl_2(B,v')$ resonance state is obtained.

Vibrational distributions of the Cl_2 product fragment were computed as described in previous works.[5,24,25] In brief, the probability $P_v(t)$ of $Cl_2(B,v)$ fragments in $v=v'-1$, $v'-2$, $v'-3$, is calculated by accumulating probability in the region of the products $Cl_2(B,v)+He$, $R>R_c=15$ a.u. (including the absorption region), in which the vdW bond can be considered broken. Then, the normalized probabilities $P_v^{norm}(t)=P_v(t)/\Sigma_v P_v(t)$ converge, after a few picoseconds, to constant values which are reliable estimates for the final vibrational populations of the $Cl_2(B,v)$ fragment.

Rotational state distributions of the $Cl_2(B,v,j)$ product fragment are calculated as the asymptotic $t\rightarrow\infty$ limit of

$$P_{v,j}(E,t)=\left|\int_{R_a}^{R_b}\left(\frac{\mu_{He-Cl_2}}{2\pi k_{v,j}\hbar^2}\right)^{1/2} e^{-ik_{v,j}R}C_{v,j}(R,t)dR\right|^2, \qquad (9)$$

where μ_{He-Cl_2} is the reduced mass associated with the R coordinate, $k_{v,j}=[2\mu_{He-Cl_2}(E-E_v^{(j)})]^{1/2}$, and E is taken to be the mean energy of the system, which is very close to the resonance energy. The limits of the integral are $R_a=15$ a.u. and $R_b=28$ a.u.

It should be noted that using the states $\chi_v^{(j)}$ in the wave packet expansion of Eq. (8), instead of the states $\chi_v^{(j=0)}$ as typically done in wave packet studies of predissociation of vdW complexes,[5,21] has two advantages. On the one side, the basis set on which the wave packet is expanded is more adapted to the system described, which benefits the wave packet propagation. On the other side, it allows a correct calculation of $k_{v,j}$ (in the case of the $\chi_v^{(j=0)}$ basis functions $E_v^{(j)}$ is approximated as $E_v^{(j)}\simeq E_v^{(j=0)}+j(j+1)\hbar^2\langle\chi_v^{(j)}\times(r)|r^{-2}|\chi_v^{(j)}(r)\rangle/2\mu_r$), and therefore, a more correct calculation of the diatomic fragment rotational state distributions.

TABLE II. Experimental and calculated spectral blueshifts with the present potential surface and with the previous UCCSD(T) and μGA surfaces. The $He–Cl_2(B,v')$ ground resonance energies (relative to the initial Cl_2 vibrational energy level) calculated with the present potential are listed in the second column.

		Blueshift (cm^{-1})			
v'	E_{res} (cm^{-1})	UCCSD(T)[a]	μGA[a]	This work	Expt.[a]
8	−11.31	3.11	3.54	3.54	3.49
9	−11.27	3.18	3.55	3.58	3.55
10	−11.23	3.34	3.60	3.62	3.65
11	−11.17	3.61	3.69	3.68	3.72
12	−11.10	3.97	3.81	3.75	3.77

[a]Reference 14.

III. RESULTS AND DISCUSSION

A. Comparison with experimental data and previous surfaces

The resonance energies of the $He–Cl_2(B,v')$ complex (or equivalently, the dissociation energy $D_0(B,v')=-E_{res}$) obtained with the present potential surface are listed in Table II for the vibrational excitations $v'=8-12$. The calculated blueshifts are also shown in the table, along with the experimental ones and those obtained with the *ab initio* UCCSD(T) and semiempirical μGA surfaces reported in Ref. 14, for the sake of comparison. Same as in Ref. 14, the value of the dissociation energy in the X electronic state,[11] $D_0(X,v''=0)=14.85$ cm^{-1}, has been used to calculate the blueshifts. The agreement of the present blueshifts with the measured

TABLE III. Experimental and calculated vibrational predissociation lifetimes with the present potential and with the previous UCCSD(T) and μGA surfaces.

	VP lifetime (ps)			
v'	UCCSD(T)[a]	μGA[a]	This work	Exp.[a]
8	152	363	450	506
9	129	268	297	275
10	109	202	192	179
11	93	155	122	97
12	74	120	78	52

[a]Reference 14.

ones is excellent in all the range of vibrational levels, with a deviation typically of ~1%. This level of accuracy, within experimental precision, is similar to that achieved with the fitted μGA surface, and superior to the description of the blueshifts provided by the UCCSD(T) potential surface.

In Table III predissociation lifetimes obtained with the current empirical He–$Cl_2(B)$ surface are collected and compared to experimental lifetimes and previously calculated ones with the UCCSD(T) and μGA surfaces, in the range $v'=8-12$. Global agreement of the present lifetimes with the experimental ones is quite good in the whole range of vibrational levels. This is particularly true for the $v'=8,9,10$ lifetimes, which deviate 11, 8, and 7%, respectively, from the measured values. For these three vibrational levels the description of the lifetime given by the current empirical surface is better than that provided by the UCCSD(T) and μGA surfaces, and also by the previous empirical potentials.[2,3] For the higher $v'=11,12$ levels the discrepancy of the present lifetimes with experimental data is larger than for the lower levels, but still the current surface yields a better agreement than the μGA and earlier empirical surfaces. It is noted that for $v'=11,12$ the best correspondence with experiment is obtained with the UCCSD(T) surface, and the lifetimes reported here for these two levels are not far from the UCCSD(T) values.

Thus, the proposed surface improves over previous potential surfaces on the description of the complex VP lifetime in the entire range of vibrational excitations $v'=8-12$, i.e., improvement in reproducing the lifetime of the lowest levels is not made at the expense of the lifetime description for the highest levels, and *vice versa*. Such an improvement is more remarkable if we take into account the difficulty of the different He–$Cl_2(B)$ potential surfaces previously proposed (empirical, semiempirical, and *ab initio*) in achieving agreement with the measured lifetimes for all the Cl_2 vibrational excitations. This comes to support the validity of the present potential, at least in the range of vibrational levels where it is tested with available experimental data.

The vibrational distribution of the $Cl_2(B,v)$ product from He–$Cl_2(B,v'=12)$ predissociation found with the present surface is 93.4% for $\Delta v'=-1$, 6.2% for $\Delta v'=-2$, and 0.4% for $\Delta v'=-3$. These results compare very favorably with the experimental values 94%, ~5%, and <1% for $\Delta v'=-1$, -2, and -3, respectively. Similar results were found with the UCCSD(T) surface, 5.9% and 0.8% for the $\Delta v'=-2$ and -3 channels, respectively, and with the μGA surface, 4.0% and 0.2% for the $\Delta v'=-2$ and -3 channels, respectively.

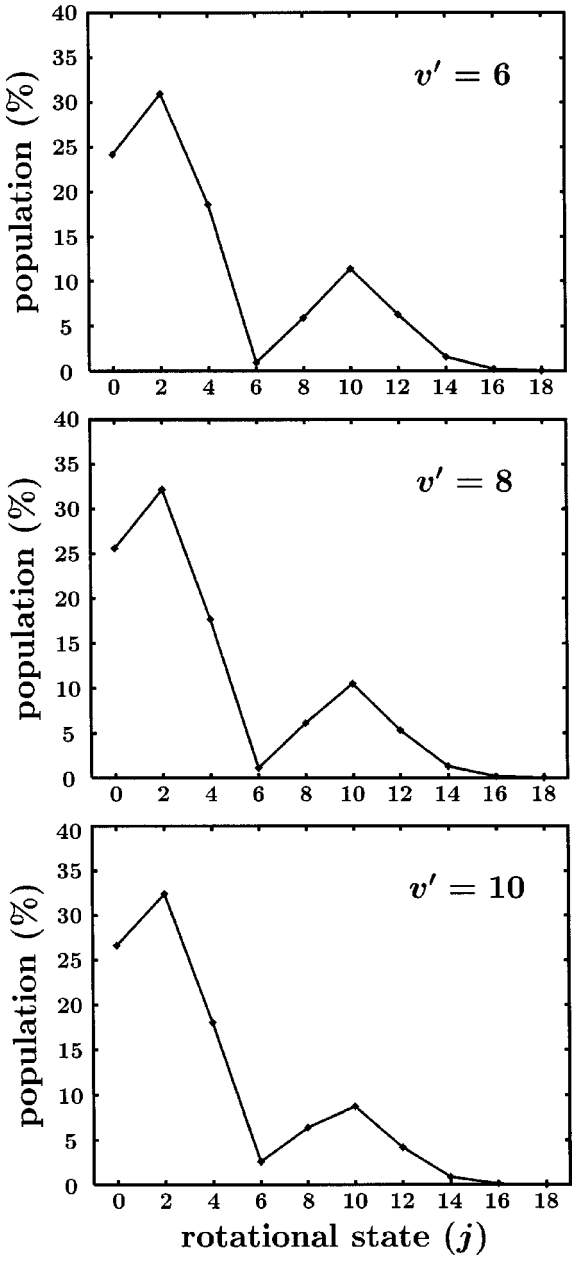

FIG. 2. Calculated Cl_2 rotational state distributions for the dissociation of He–$Cl_2(B,v'=6,8,10)$ through the $\Delta v'=-1$ vibrational channel.

Rotational state distributions of the $Cl_2(B,v=v'-1,j)$ fragment calculated with the present potential surface are displayed in Fig. 2 for $v'=6$, 8, and 10. Similarly, the rotational distributions corresponding to the channels $\Delta v'=-1$, -2, and -3 of the vibrational level $v'=12$ are shown in Fig. 3. The distributions reported here can be compared with the measured ones and those obtained with the UCCSD(T) and μGA surfaces, which are presented in Figs. 7 and 8 of Ref. 14. In general, the experimental rotational distributions are well reproduced by the previous He–$Cl_2(B)$ surfaces.[2,14] The present distributions of Fig. 2 are also in good agreement with the experimental ones, and show a level of accuracy similar to that obtained with the UCCSD(T) and μGA surfaces (see Fig. 7 of Ref. 14). The

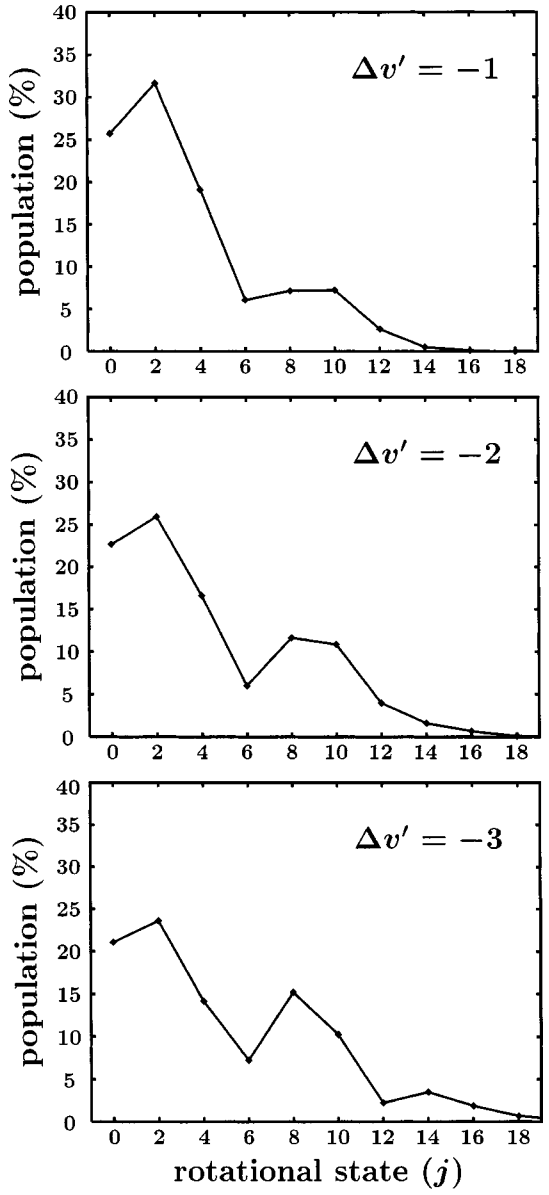

FIG. 3. Calculated Cl_2 rotational state distributions for the dissociation of $He–Cl_2(B,v'=12)$ through the $\Delta v'=-1$, -2, and -3 vibrational channels.

bimodality of the distributions, the positions of the peaks and nodes, and even the population of most of the rotational states are quite well reproduced. The largest discrepancy with experiment is observed in the overestimated population of $j=0$ in the $v'=10$ distribution, similar to the result predicted by the UCCSD(T) and μGA surfaces.

The calculated rotational distributions for the three vibrational predissociation channels of $v'=12$ (Fig. 3) present some improvements with respect to the corresponding distributions obtained with the UCCSD(T) and μGA surfaces (see Fig. 8 of Ref. 14). Very good agreement is found between the present $\Delta v'=-1$ distribution and the experimental one. The populations of $j=8$ and 10, although slightly underestimated, are closer to the experimental values than the UCCSD(T) and μGA results. The $\Delta v'=-2$ and -3 distributions are also globally closer to the measured distributions. In particular, the present $\Delta v'=-2,-3$ distributions predict the experimental j value, $j=8$, of the second peak of the distribution, while this peak occurs at $j=10$ with the UCCSD(T) and μGA surfaces. In addition, the intensity of the node at $j=6$ in the three distributions of Fig. 3 is closer to the corresponding experimental population than the UCCSD(T) and μGA results. The $\Delta v'=-3$ distribution of Fig. 3 also reproduces the small third maximum at $j=14$. This maximum is predicted by the μGA surface but not by the UCCSD(T) one. It is stressed that the populations associated with the $\Delta v'=-2$ and -3 vibrational channels are 6.2% and 0.4%, respectively. With such small populations, the present empirical potential surface is able to describe the details of the experimental rotational distributions (particularly in the $\Delta v'=-3$ channel).

B. Range of validity of the potential surface

Usually the validity of an empirical potential is rather limited to the regions probed by the experimental data used to fit the potential parameters. In the case of $He–Cl_2(B)$ those regions correspond essentially to the $v'=8-12$ vibrational levels of Cl_2 (for $v'=6$ there are less experimental data available). As shown in Sec. III A, the present surface provides a good description of the spectroscopy and dynamics of the complex in this range of vibrational excitations. Compared to previous potential surfaces, the current empirical fit improves significantly on the description of some properties, like the predissociation lifetime, and for the remaining properties it provides at least the same level of quality as the best one achieved by the earlier surfaces. This assesses the reliability of the potential in the region probed experimentally. It is interesting to have an idea of the extent to which the empirical surface can be valid beyond that region. To this purpose, in the following the potential is analyzed and compared to the *ab initio* UCCSD(T) surface.

In Fig. 4 plots of the empirical potential as a function of the $He–Cl_2$ bond distance R are shown for three Cl–Cl separations in the perpendicular configuration of the complex, $\theta=90°$. The corresponding UCCSD(T) *ab initio* curves are also shown in the figure for comparison. The *ab initio* curves are the average $V_+=(A'+A'')/2$ of the points for the A' and A'' states reported in Ref. 14. The empirical and the *ab initio* curves are similar, particularly for the case of $r=2.1$ Å. With increasing r the empirical potential becomes gradually deeper than the *ab initio* one in the R region corresponding to the short-range wall and the bottom of the well. Interestingly, for the three Cl–Cl separations, the empirical and the *ab initio* curves agree very well for R distances larger than the equilibrium one. As it has been pointed out,[14] the *ab initio* calculations are probably most accurate for these $He–Cl_2$ bond separations.

Contour plots of the $He–Cl_2(B)$ empirical surface are displayed in Fig. 5 for $r=2.1$, 2.4, and 3.0 Å, which can be compared with the corresponding plots of the UCCSD(T) surface shown in Fig. 3 of Ref. 14. Again the plots of the two potential surfaces are very similar, the main difference being that the empirical potential is less repulsive at short $He–Cl_2$ distances. Such a difference would be responsible of the present improvement on the description of the blueshifts and

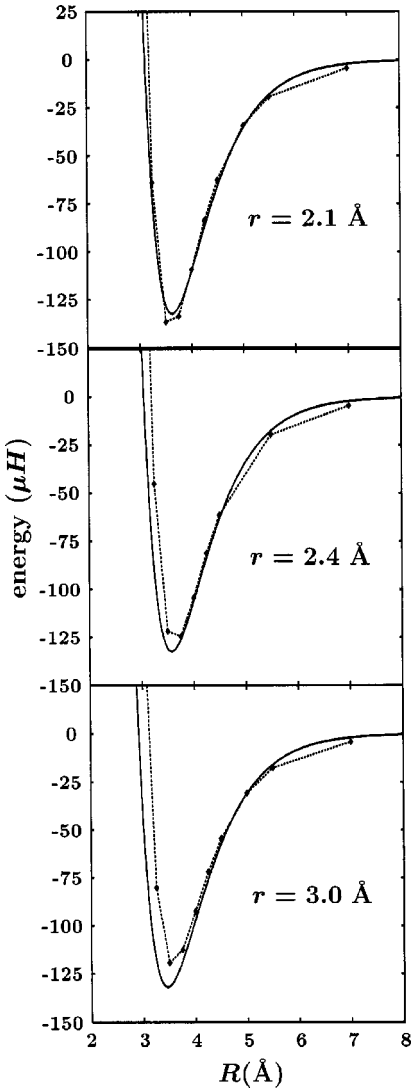

FIG. 4. Empirical potential curves vs R (solid lines) for three Cl–Cl separations, $r=2.1$, 2.4, and 3.0 Å, in the perpendicular configuration ($\theta=90°$) of the complex. The corresponding *ab initio* UCCSD(T) curves (dashed lines), reported in Tables I–VI of Ref. 14, are also shown for comparison. See the text for details.

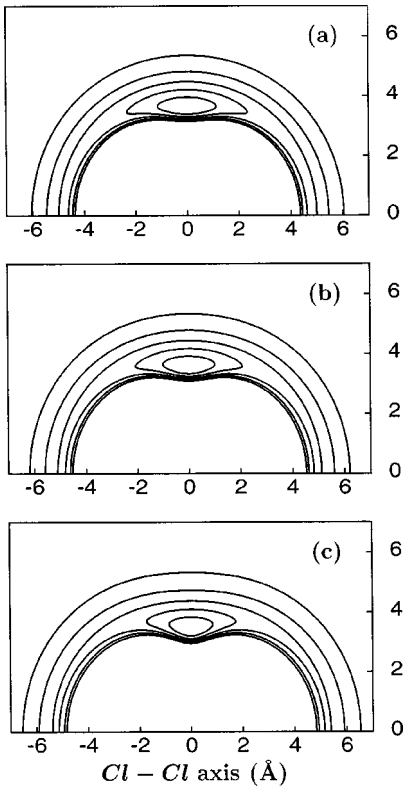

FIG. 5. Contour plots of the He–$Cl_2(B)$ empirical potential surface for three Cl–Cl separations, $r=2.1$ Å (a), $r=2.4$ Å (b), and $r=3.0$ Å (c). Spacing between the contours is 5 cm^{-1} starting from the outermost contour at -5 cm^{-1}, and the units are Å on both axis of the plot. For $r=2.1$, 2.4, and 3.0 Å, the Cl atoms are located at ±1.05 Å, ±1.2 Å, and ±1.5 Å, respectively, on the horizontal axis of the plot.

predissociation lifetimes with respect to the UCCSD(T) results.

Some features of the empirical surface, like the energy and position of the potential minimum in the linear and perpendicular configurations of He–$Cl_2(B)$, are listed in Table IV for several Cl–Cl separations. For the $r=2.1$, 2.4, and 3.0 Å distances, the values of Table IV can be compared with those reported in Table VIII of Ref. 14 for the UCCSD(T) surface. In the perpendicular configuration, the energy and position of the potential minimum are close to those of the *ab initio* surface ($V_+^{\min}=-29.65$, -28.29, and -26.77 cm^{-1}, and $R^{\min}=3.56$, 3.64, and 3.58 Å for $r=2.1$, 2.4, and 3.0 Å, respectively). In the linear configuration similar agreement is found for the equilibrium positions at the three Cl–Cl separations, and for the minimum energy at $r=2.1$ Å, while for $r=2.4$ and 3.0 Å the *ab initio* potential minima are about 5 cm^{-1} deeper than the present ones.

In the range 2.1 Å$\leqslant r\leqslant$4.0 Å Table IV shows that with increasing r, $R^{\min}(\theta=0°)$ increases and $R^{\min}(\theta=90°)$ decreases monotonically. For both the linear and the perpendicular configurations $V^{\min}$ decreases when r increases, slowly for $r<3.0$ Å and more rapidly for $r>3.0$ Å. This behavior is related to the decrease of $\epsilon(r)$ and $\alpha(r)$ for $r>r^*=2.9$ Å. For $r>3.5$ Å the potential minimum vanishes quickly for both the linear and perpendicular configurations, and the onset of nonphysical behavior appears (which becomes more clear for $r>4.0$ Å). Apparently the decrease of $\epsilon(r)$ and $\alpha(r)$ is too fast for Cl–Cl distances $r>3.5$ Å. Thus, the present empirical surface does not describe the correct asymptotic behavior for large Cl–Cl distances, and the upper limit of its range of validity would be $r\sim3.5$ Å, or equivalently $v'=13,14$. This range could be increased by changing the functional form of $\epsilon(r)$ and $\alpha(r)$ for large Cl–Cl separations. A possibility would be that $\epsilon(r)$ and $\alpha(r)$ decrease more slowly for $r>3.5$ Å, but additional experimental data probing this region would be required in order to carry out a realistic fit. Concerning the lower limit of the empirical surface, it is estimated that it can provide a reliably good description of the spectroscopy and dynamics up to $v'=6$, and this description will gradually deteriorate for lower vibrational levels.

IV. CONCLUSIONS

An empirical potential surface for the He–$Cl_2(B\,^3\Pi_u)$ complex is proposed. The interaction surface is modeled as a

TABLE IV. Energies and positions of the potential minima in the linear ($\theta=0°$) and perpendicular ($\theta=90°$) configurations of He–$Cl_2(B)$ for several Cl–Cl separations.

	$r=2.1$ Å	$r=2.4$ Å	$r=3.0$ Å	$r=3.5$ Å	$r=4.0$ Å
$V^{min}(\theta=0°)$ (cm^{-1})	−15.93	−15.44	−14.87	−12.98	−9.05
$V^{min}(\theta=90°)$ (cm^{-1})	−29.04	−29.04	−28.95	−25.27	−16.24
$R^{min}(\theta=0°)$ (Å)	4.79	4.95	5.26	5.51	5.70
$R^{min}(\theta=90°)$ (Å)	3.62	3.57	3.46	3.34	3.20

sum of an intramolecular Cl_2 potential (represented by a Morse function) plus an intermolecular He–Cl_2 potential. The intermolecular He–Cl_2 interaction is represented by additive pairwise potentials, and involves only six parameters. The main novelty of the present He–$Cl_2(B)$ intermolecular potential with respect to previous empirical surfaces, is that a dependence on the Cl–Cl separation is introduced for some of the parameters. This makes more flexible the simple form of additive atom–atom potentials used. The six parameters of the intermolecular potential are fitted in order to reproduce the available measurements of several spectroscopic and dynamical properties in the range $v'=8-12$ (and, to a lesser extent, for $v'=6$) of Cl_2 vibrational excitations. Such properties include spectral blueshifts, predissociation lifetimes, and vibrational and rotational Cl_2 product state distributions.

The present potential is found to improve significantly on the description of the predissociation lifetimes in the whole $v'=8-12$ range, as compared to previous He–$Cl_2(B)$ surfaces. In addition, the spectral blueshifts are reproduced within experimental precision for all the vibrational levels. As shown in earlier works, an accurate description of these two properties (and in particular of the lifetime) involves special difficulties in the case of He–$Cl_2(B)$, due to the delocalized nature of this system. The present surface reproduces the Cl_2 vibrational and rotational distributions with a level of quality similar (or even better in some cases) to the best one achieved by the previous surfaces. Thus, the reported He–$Cl_2(B)$ empirical potential provides the best global description to date of the spectroscopic and dynamical properties in the range of vibrational excitations where measurements are available. The improvement achieved is related, to a large extent, to the dependence on the Cl–Cl separation introduced in some of the potential parameters. The range of validity of the empirical potential has been analyzed, and it is found to be rather limited to the region probed experimentally (i.e., in the range 2.0–3.5 Å of Cl–Cl separations). A possibility to increase this range of validity to other regions is suggested, subject to the availability of additional experimental data for those regions.

ACKNOWLEDGMENTS

Helpful discussions with Dr. R. Prosmiti are acknowledged. This work was supported by C.I.C.Y.T. (Ministerio de Ciencia y Tegnología), Spain, Grant No. BFM-2001-2179, and by the European network TMR Grant No. HPRN-CT-1999-00005.

[1] J. I. Cline, N. Sivakumar, D. D. Evard, C. R. Bieler, B. P. Reid, N. Halberstadt, S. R. Hair, and K. C. Janda, J. Chem. Phys. **90**, 2605 (1988).
[2] J. I. Cline, B. P. Reid, D. D. Evard, N. Sivakumar, N. Halberstadt, and K. C. Janda, J. Chem. Phys. **89**, 3535 (1988).
[3] L. Beneventi, P. Casavecchia, G. G. Volpi, C. R. Bieler, and K. C. Janda, J. Chem. Phys. **98**, 178 (1993).
[4] A. Rohrbacher, K. C. Janda, L. Beneventi, P. Casavecchia, and G. G. Volpi, J. Phys. Chem. A **101**, 6528 (1997).
[5] A. García-Vela, J. Phys. Chem. A **106**, 6857 (2002).
[6] S. S. Huang, C. R. Bieler, F.-M. Tao, W. Klemperer, P. Casavecchia, G. G. Volpi, N. Halberstadt, and K. C. Janda, J. Chem. Phys. **102**, 8846 (1995).
[7] A. Rohrbacher, J. Williams, K. C. Janda, S. M. Cybulski, R. Burcl, M. M. Szczęśniak, G. Chalasiński, and N. Halberstadt, J. Chem. Phys. **106**, 2685 (1997).
[8] J. Williams, A. Rohrbacher, D. Djahandideh, K. C. Janda, A. Jamka, F.-M. Tao, and N. Halberstadt, Mol. Phys. **91**, 573 (1997).
[9] F. Y. Naumkin and F. R. W. McCourt, J. Chem. Phys. **108**, 9301 (1998).
[10] F. Y. Naumkin and F. R. W. McCourt, J. Chem. Phys. **109**, 1271 (1998).
[11] S. M. Cybulski and J. S. Holt, J. Chem. Phys. **110**, 7745 (1999).
[12] G. Chalasiński, M. Gutowski, M. M. Szczęśniak, J. Sadlej, and S. Scheiner, J. Chem. Phys. **101**, 6800 (1994).
[13] S. M. Cybulski, R. Burcl, G. Chalasiński, and M. M. Szczęśniak, J. Chem. Phys. **103**, 10116 (1995).
[14] J. Williams, A. Rohrbacher, J. Seong *et al.* J. Chem. Phys. **111**, 997 (1999).
[15] F.-M. Tao and W. Klemperer, J. Chem. Phys. **97**, 440 (1992).
[16] F. Y. Naumkin and F. R. W. McCourt, J. Chem. Phys. **107**, 5702 (1997).
[17] F. Y. Naumkin, Chem. Phys. **226**, 319 (1998).
[18] C. F. Kunz, I. Burghardt, and B. A. Heß, J. Chem. Phys. **109**, 359 (1998).
[19] J. I. Cline, D. D. Evard, and K. C. Janda, J. Chem. Phys. **84**, 1165 (1986).
[20] N. Halberstadt, J. A. Beswick, and K. C. Janda, J. Chem. Phys. **87**, 3966 (1987).
[21] S. K. Gray and C. E. Wozny, J. Chem. Phys. **91**, 7671 (1989).
[22] H. Tal-Ezer and R. Kosloff, J. Chem. Phys. **81**, 3967 (1984).
[23] V. Engel, Chem. Phys. Lett. **189**, 76 (1992).
[24] M. Ceotto and A. García-Vela, J. Chem. Phys. **115**, 2146 (2001).
[25] F. Le Quéré and S. K. Gray, J. Chem. Phys. **98**, 5396 (1993).